Bull. Mater. Sci. (2018) 41:134
https://doi.org/10.1007/s12034-018-1650-y

Effect of CTAB coating on structural, magnetic and peroxidase mimic activity of ferric oxide nanoparticles

DIKSHIT GARG[1,*], MANPREET KAUR[1], SUCHETA SHARMA[2] and VIBHA VERMA[1]
[1]Department of Chemistry, Punjab Agricultural University, Ludhiana 141004, Punjab, India
[2]Department of Biochemistry, Punjab Agricultural University, Ludhiana 141004, Punjab, India
*Author for correspondence (dikshitgarg762@gmail.com)

MS received 10 May 2018; accepted 20 August 2018; published online 4 October 2018

Abstract. In the present work, pristine and cetyl trimethyl ammonium bromide (CTAB)-coated ferric oxide nanoparticles (CTAB@Fe_2O_3 NPs) were synthesized and studied as enzyme mimics. The w/w ratio of Fe_2O_3 to CTAB was varied as 1:1 and 1:2. Transmission electron microscopic analysis revealed that pristine NPs had an average size of 50 nm, whereas the presence of CTAB resulted in the formation of nanorods with length of 130 nm. BET studies confirmed enhancement of surface area on CTAB coating, which was maximum for w/w ratio 1:1. The synthesized pristine NPs and CTAB-coated NPs were evaluated for their peroxidase mimic activity using o-dianisidine dihydrochloride as substrate. Optimum pH, temperature, substrate and NPs concentration for the reaction were 1, 25°C, 0.16 mg ml^{-1} and 1 mg ml^{-1}, respectively. Peroxidase mimic activity of CTAB@Fe_2O_3 NPs (w/w 1:1) was higher than that of pristine NPs. However, further increase in CTAB coating (w/w 1:2) resulted in lowering of peroxidase mimic activity. Kinetic analysis was carried out at optimized conditions; maximum velocity (V_{max}) and Michaelis constant (K_m) value of CTAB@Fe_2O_3 NPs at 1:1 w/w ratio were 7.69 mM and 1.12 μmol s^{-1}, respectively.

Keywords. Ferric oxide nanoparticles; peroxidase enzyme; enzyme mimic; CTAB.

1. Introduction

Artificial enzymes have been attracting the attention of researchers due to several disadvantages in the performance of natural enzymes such as rapid denaturation by environmental changes, which alter their structure and catalytic properties [1]. Preparation, purification and storage of natural enzymes are very difficult, expensive and time-consuming, which limits their widespread applications [2]. Artificial enzymes, on the contrary, have been explored because of their easy preparation, low-cost storage and purification processes [3]. Nanomaterials as enzyme mimics have become a growing area of research. Thus, it is crucial to look for stability, catalytic efficiency and enzyme mimic activity from the practical point of view. They have already gained several applications in the fields such as immunoassays, therapy, stem cell growth, pollutant removal and cancer diagnostics [4]. To date, several artificial enzymes have been reported to mimic natural analogues, including hydrolase, aldolase, nitrile hydratase, ligase, lipase, peroxidase and superoxide dismutase [5,6].

A variety of nanostructures, including carbon materials [7–9], nanocomposites [10,11], noble metals [12,13] and metal oxides [14–16], have displayed peroxidase-like activity. Of late, magnetic nanoparticles (NPs) have become rapidly growing and most exciting areas for studying peroxidase mimic activity. Fe_2O_3 NPs are reported to exhibit enhanced peroxidase mimic activity as compared with natural horseradish peroxidase (HRP) [17]. These NPs have the ability of scavenging or generating reactive oxygen species that can be used to mimic the peroxidase activity of natural ones. Similar to HRP, Fe_2O_3 NPs catalyse the oxidation of various substrates such as 3,3,5,5,-tetramethylbenzidine (TMB), o-phenylenediamine (OPD), 3,3-diaminobenzidine (DAB) and o-dianisidine dihydrochloride. All substrates undergo differential colour change when catalytically oxidized on exposure to Fe_2O_3 NPs. To date, a number of peroxidase mimic NPs, including maghemite, magnetite and enzymes containing Fe^{2+} and Fe^{3+} in their reaction centre, have been explored [18–21].

Activity of Fe_2O_3 gets altered on coating. Citrate-capped Fe_2O_3 NPs (N_{cit}) showed higher turnover value as compared with caboxymethyl dextrane (K_{CMD})-coated NPs with both TMB and ABTS [2,2′-azino-bis(3-ethylbenzothiazoline-6-sulphonic acid)] as substrate. A possible reason for the low activity of K_{CMD} was its thicker coating that resulted in the steric effects. On the other hand, glycerine-coated ferric oxide NPs (N_{gly}) displayed higher K_{cat} value than polylysine-coated ferric oxide NPs (N_{PLL}) towards TMB but displayed low K_{cat} value towards ABTS. N_{PLL} have a slightly higher positive charge present on their surface than N_{gly}, which affects the activity [22].

Several other NPs have been reported, such as Fe_2O_3 NPs coated with both high molecular mass and low molecular mass dextran [23–26], iron NPs coated with carboxyl dextran [27–29], silica-coated super-paramagnetic iron oxide NPs [30,31] and non-stoichiometric super-paramagnetic Fe_2O_3 NPs coated with polyglucose orbital carboxymethyl ether [32]. Cetyl trimethyl ammonium bromide (CTAB) surfactant is mostly used in the preparation of NPs due to its property of controlling the shape and size of the particles [33,34]. To the best of our knowledge, peroxidase mimic activity of CTAB-coated Fe_2O_3 NPs has not been reported. In the present work, cationic CTAB was chosen as surfactant for Fe_2O_3 NPs coating because it can interact with the negatively charged iron oxide NPs formed during co-precipitation. Effect of changing CTAB coating on the peroxidase mimic activity of Fe_2O_3 NPs has also been studied using o-dianisidine dihydrochloride as substrate.

2. Experimental

2.1 *Synthesis and characterization*

All chemicals used, i.e., hydrogen peroxide ($H_2O_2 - 30\%$), NH_4OH (wt. 25%), CTAB ($C_{19}H_{42}BrN$), ferrous ammonium sulphate [$(NH_4)_2Fe(SO_4)_2 \cdot 6H_2O$], ammonium ferric sulphate [$NH_4Fe(SO_4)_2 \cdot 6H_2O$], o-dianisidine dihydrochloride [$C_{14}H_{18}Cl_2N_2O_2$] were of analytical reagent grade. Pristine and CTAB-coated Fe_2O_3 NPs (with varying w/w ratio of Fe_2O_3 : CTAB, i.e., 1:1 and 1:2) were synthesized by co-precipitation method; these NPs were designated as F-1, F-2 and F-3, respectively. To synthesize pristine Fe_2O_3 NPs, 0.022 mol of [$NH_4Fe(SO_4)_2 \cdot 6H_2O$] and 0.0146 mol of $(NH_4)_2Fe(SO_4)_2 \cdot 6H_2O$ were dissolved in 50 ml de-ionized water with continuous stirring [35]. In order to form precipitates, 5 ml ammonium hydroxide was added to this solution dropwise with vigorous stirring until the pH of the mixture reached up to 9. This solution was further stirred for 45 min with continuous heating at 85°C. Precipitates formed were separated by centrifugation. Filtrate was washed with ethanol followed by de-ionized water several times until the pH of the filtrate became 7. Filtrate was dried in an oven at 100°C for 8 h. Similar method was employed for the synthesis of CTAB@Fe_2O_3 NPs. During synthesis of Fe_2O_3 NPs, CTAB was added in w/w ratio of 1:1 and 1:2 in the reaction mixture and CTAB-coated Fe_2O_3 NPs were labelled as F-2 and F-3, respectively.

The Scherrer relationship was applied to find the average particle size:

$$D = 0.9\lambda/\beta\cos\theta,$$

where λ represents wavelength of X-ray (1.54 nm), β represents full-width at half-maximum (FWHM) and θ is diffraction angle (17.866°). Details of techniques employed, viz., FT-IR, X-ray diffraction (XRD), scanning electron microscopy (SEM), transmission electron microscopy (TEM), VSM and BET analysis are described in the previous publication [36].

2.2 *Kinetic analysis*

Enzyme mimic activity of synthesized NPs was evaluated by the method of Shannon *et al* [37]; pH of the reaction mixture was varied from 1 to 10 using 0.1 N HCl and 0.1 N NaOH to ascertain optimum pH. Effect of catalyst dose, substrate concentration, temperature and contact time was studied to optimize the reaction conditions. Kinetic experiments were carried out under optimized conditions. The solution was analysed at 430 nm using a UV–vis spectrophotometer in time course mode for 3 min, with a 30-s time interval. The Lineweaver–Burk plot was employed for the calculation of Michaelis–Menten constant as follows:

$$\frac{1}{\nu} = \frac{K_m}{V_{max}\,((1/[S]) + (1/K_m))}.$$

Here, ν is initial velocity, V_{max} and [S] represent the maximum velocity of the reaction and substrate concentration, respectively, whereas K_m represents the Michaelis–Menten constant, which is an indicator of enzyme affinity for its substrate. Smaller the value of K_m, greater the affinity between enzyme and substrate.

3. Characterization

3.1 *Structural analysis*

The crystalline structure of F-1, F-2 and F-3 was identified by the XRD technique. Diffraction peaks in XRD (figure 1a) pattern of Fe_2O_3 NPs were observed at 2θ = 20, 30.39, 35.73, 43.42, 53.81, 57.39 and 63.01° with the inter-planar spacing of 0.29, 0.25, 0.20, 0.17, 0.16 and 0.16 nm, which were assigned to (111), (104), (110), (202), (116), (018) and (214) planes, respectively. These data matched with the values reported in literature for Fe_2O_3 NPs [38]. In F-2 and F-3, the peaks were broadened and increase in FWHM was observed, which confirmed decrease in average particle size as compared with bare Fe_2O_3 NPs. These results suggested that the inter-planar spacing increased, which led to the decrease in particle size.

The binding of CTAB to the Fe_2O_3 NPs was investigated by FT-IR spectra. Figure 1b presents the IR spectra of pristine and CTAB-coated Fe_2O_3 NPs. In pristine Fe_2O_3 NPs, the bands at 1582 and 3172 cm^{-1} are attributed to O–H bending and stretching vibrations, respectively, which is due to the water molecules adsorbed onto the surface of bare NPs. Absorption bands in the region of 415–618 cm^{-1} are assigned to Fe–O stretching vibrations

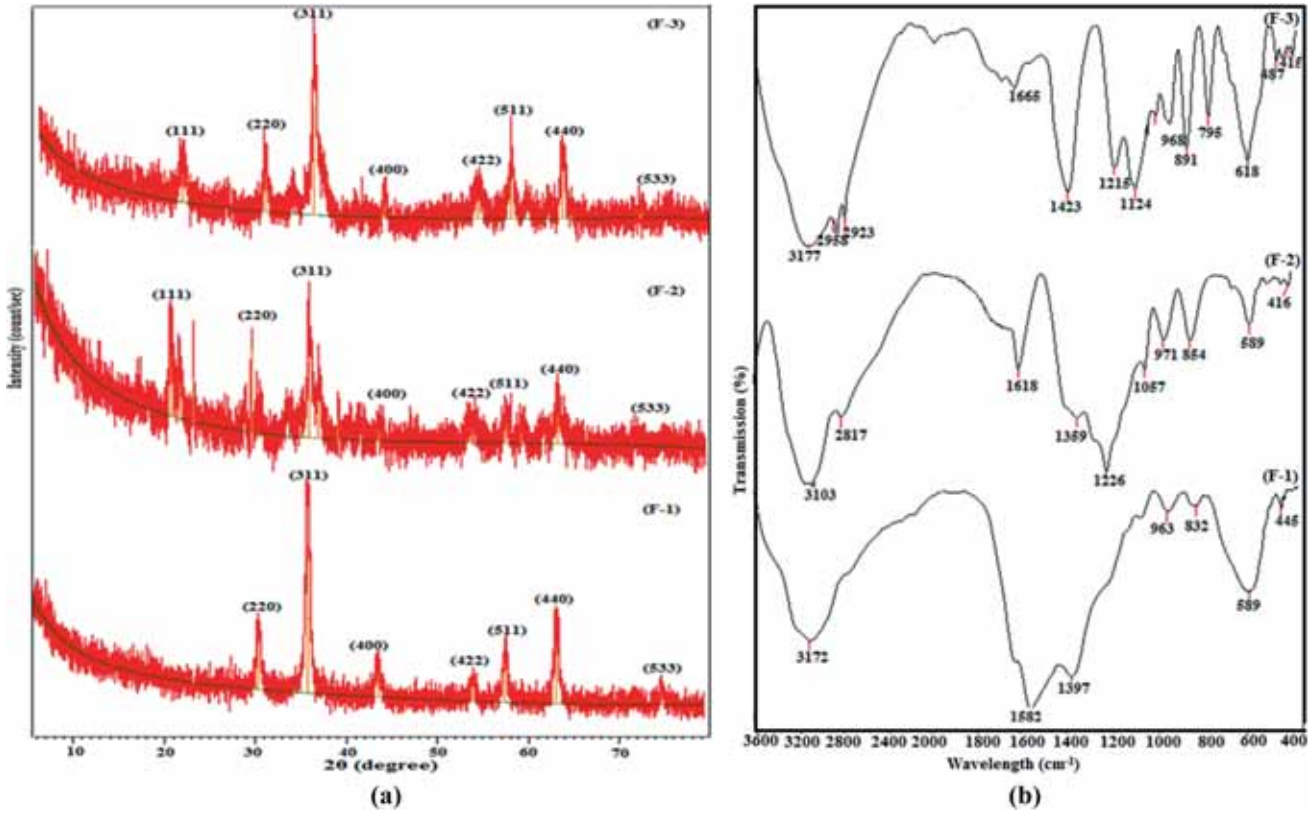

Figure 1. **(a)** XRD patterns and **(b)** FT-IR graphs of bare and CTAB-coated Fe_2O_3 NPs.

[39]. The absorption bands at 445 cm^{-1} in bare NPs and 416, 487 cm^{-1} in the surfactant-coated NPs are due to Fe–O bond vibrations in octahedral sites. The bands at 589 cm^{-1} in bare NPs and at 586, 618 cm^{-1} in CTAB-coated NPs correspond to Fe–O bond vibrations in the tetrahedral sites. In case of bare and CTAB-coated Fe_2O_3 NPs, the bands at 3172, 3103 and 3177 cm^{-1} correspond to O–H stretching vibrations. Furthermore, the bands at 1124, 1215 and 1226 cm^{-1} in CTAB-coated NPs correspond to C–N bond stretching. The bands at 1359 and 1423 cm^{-1} are due to the residual ammonia used at the time of NPs preparation.

Furthermore, the bands at 1665 and 1618 cm^{-1} correspond to N–H bending vibrations, and the bands at 3177 cm^{-1} in coated NPs correspond to stretching vibrations of O–H bonds. The bands at 968, 891, 971 and 854 cm^{-1} in both types of CTAB-coated NPs are due to the presence of tertiary amine. The bands over 3000–3600 cm^{-1} are attributed to reduced amount of water present in the samples. The bands at 795 cm^{-1} correspond to C–H bending of long alkane chain present in CTAB. Furthermore, additional bands in the range of 2800–3000 cm^{-1} in coated NPs are attributed to the stretching vibrations of C–H bonds of the saturated alkane [40]. In addition, a small shift in peaks was seen on coating Fe_2O_3 NPs with CATB, which is due to the change in environment of bare NPs.

3.2 *Morphological studies*

SEM and TEM were used to study the surface morphology and particle size distribution of synthesized pristine and CTAB-coated NPs. SEM micrographs of pristine NPs (figure 2a) clearly depict their porous surface, whereas CTAB-coated NPs, F-2 and F-3 (figure 2b and c), have somewhat more porous structure as compared with F-1 due to the immobilization of CTAB onto the surface of Fe_2O_3 NPs. TEM images (figure 3) reveal shape and morphology of NPs. F-1 appeared to be spherical and somewhat agglomerated due to the strong dipole–dipole magnetic interactions between NPs. However, rods were formed when Fe_2O_3 NPs were synthesized in the presence of CTAB due to the adsorption of CTAB on the surface of NPs, thus preventing their agglomeration due to the repulsion between the similar charged ions of CTAB. Particle size of Fe_2O_3 NPs also decreased on coating CTAB.

A similar reason for the rod formation was given by Chen *et al* [41] in their study when Fe_3O_4 NPs were treated with $FeCl_3$ solution. Fe^{3+} ions were absorbed on the surface of NPs due to the common ion effect. This scheme was co-ordinated with our approach for the CTAB-coated Fe_2O_3 NPs. Another approach towards the formation of rod-shaped NPs was reported by Zhao and Nan [40]. The stability arises from the fact that a certain amount

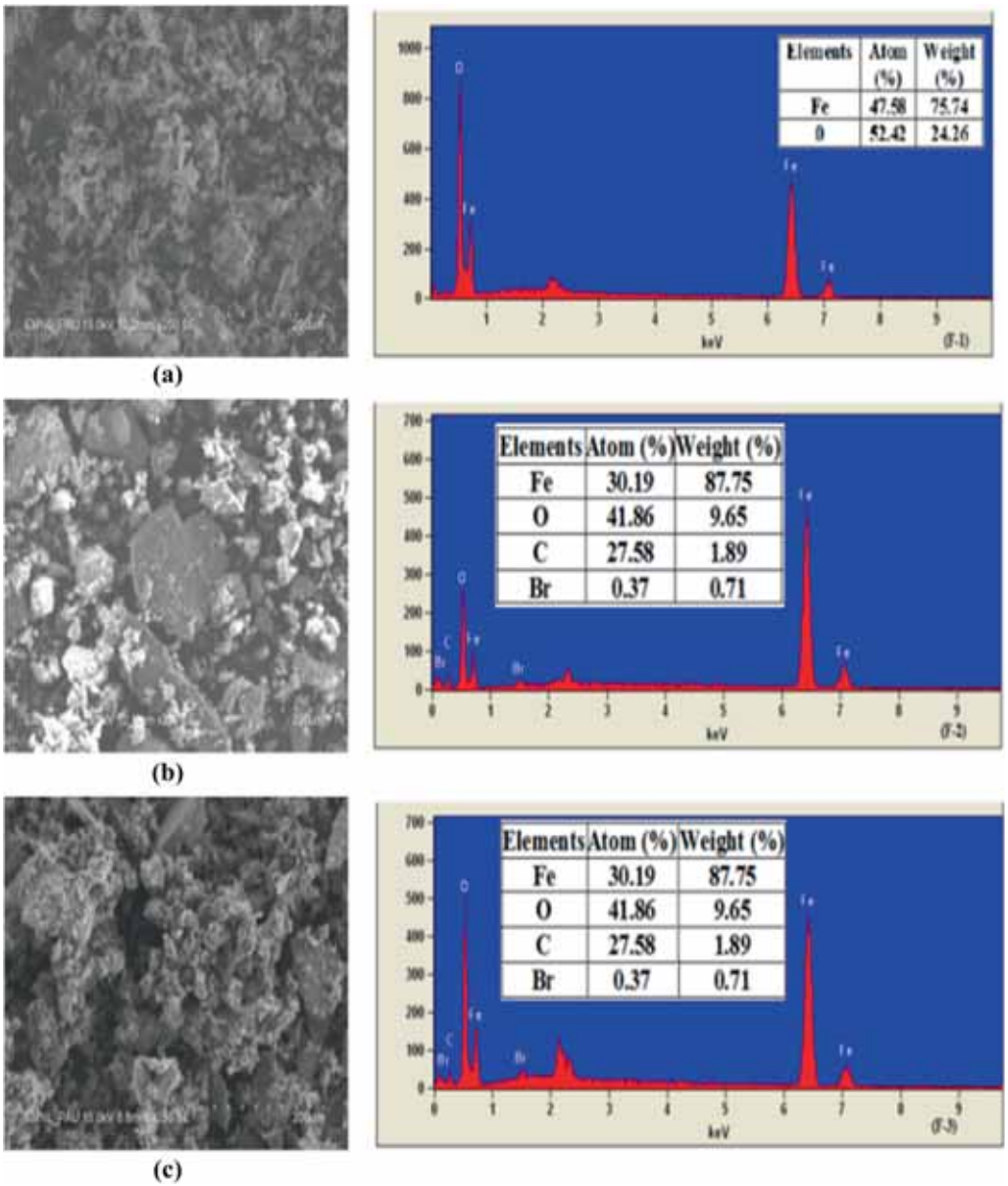

Figure 2. SEM–EDX images of (**a**) F-1, (**b**) F-2 and (**c**) F-3.

of space was occupied by the polymers coated on the surface of NPs. The space was compressed when the NPs came too close, thus triggering the formation of rod-shaped NPs.

Nitrogen adsoprtion–desorption studies of pristine and CTAB-coated Fe_2O_3 NPs were carried using BET analysis to characterize the surface properties of synthesized NPs. Figure 4 displays nitrogen sorption isotherms and pore size distribution curves. IUPAC classification designates these isotherms as type IV, which represents mesoporous structure with comparatively broad hysteresis loop belonging to H1 type. The meso-porosity of the F-2 increased with increase in the pore volume as compared with bare ones but decreased on further increase in coating. The BET surface area of F-2 and F-3 NPs was 69.174 and 49.072 m^2g^{-1}, respectively (table 1). Lower surface area of F-1 was due to the strong Van der Walls forces of interaction among particles, which led to their agglomeration.

3.3 *Magnetic studies*

Hysteresis loop depicted the effect of change in magnetic field on magnetization and magnetic flux of synthesized NPs. Variation in magnetic character of the NPs on coating with CTAB was also seen from the loop (figure 5) and the magnetic parameters of the synthesized NPs (table 2). The saturation

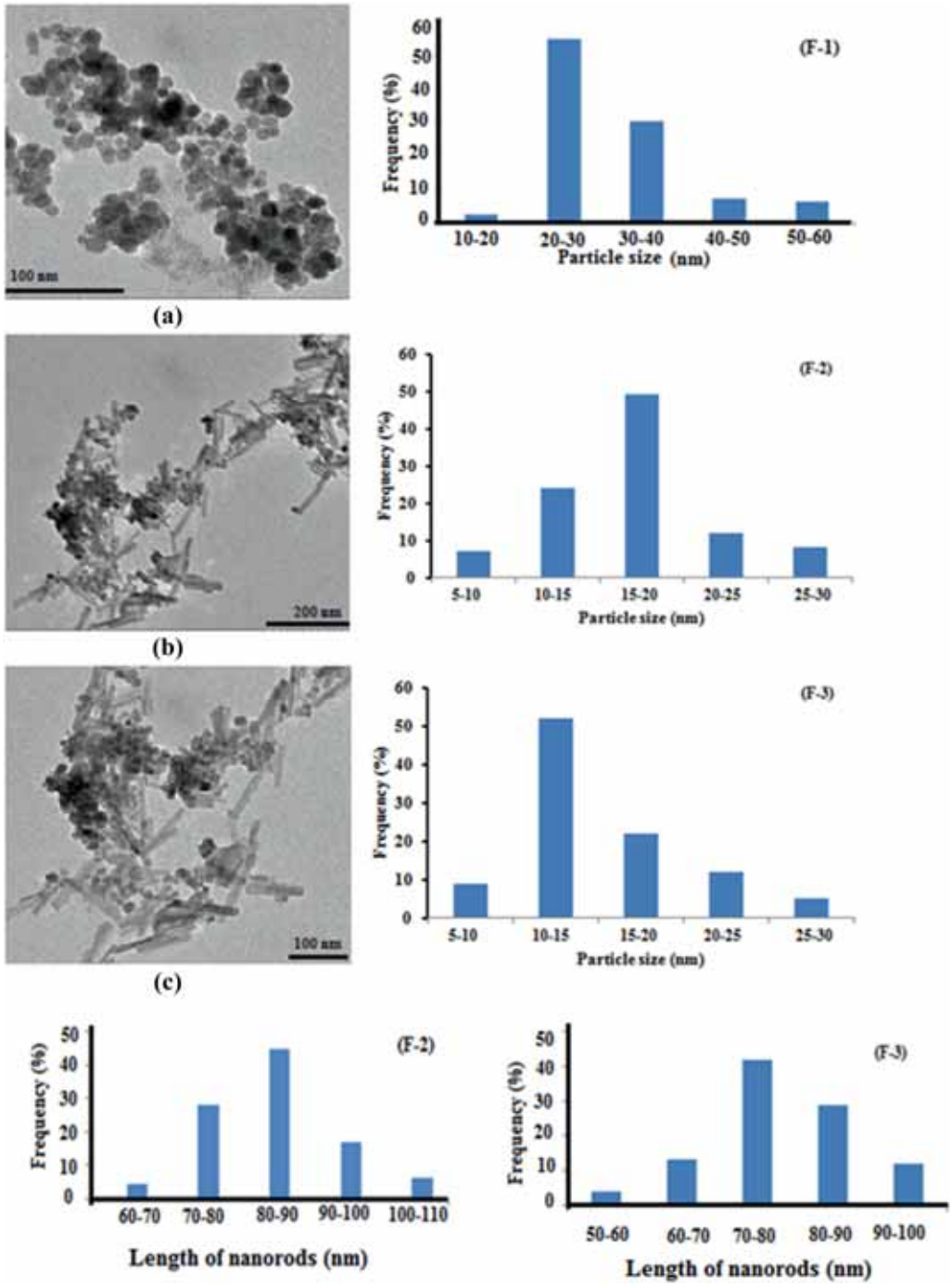

Figure 3. TEM images and histograms of (**a**) pristine NPs (F-1). CTAB@Fe_2O_3 with (**b**) 1:1 (F-2) and (**c**) 2:1 (F-3) ratio.

magnetization (M_s) of F-2 and F-3 NPs was decreased due to coating of non-magnetic CTAB on the surface of Fe_2O_3 NPs. Low coercivity values of these NPs also categorized them as soft ferromagnetic material. Narrow hysteresis loops along with low coercivity range of NPs from 12.98 to 54.05 O_e show that these NPs can be easily demagnetized [42].

4. Enzyme mimic activity of pristine and CTAB-coated Fe_2O_3 NPs

The peroxidase-like activity of synthesized NPs with o-dianisidine dihydrochloride as substrate was studied in the presence of H_2O_2. o-dianisidine dihydrochloride possessed opposite charge character than that of synthesized

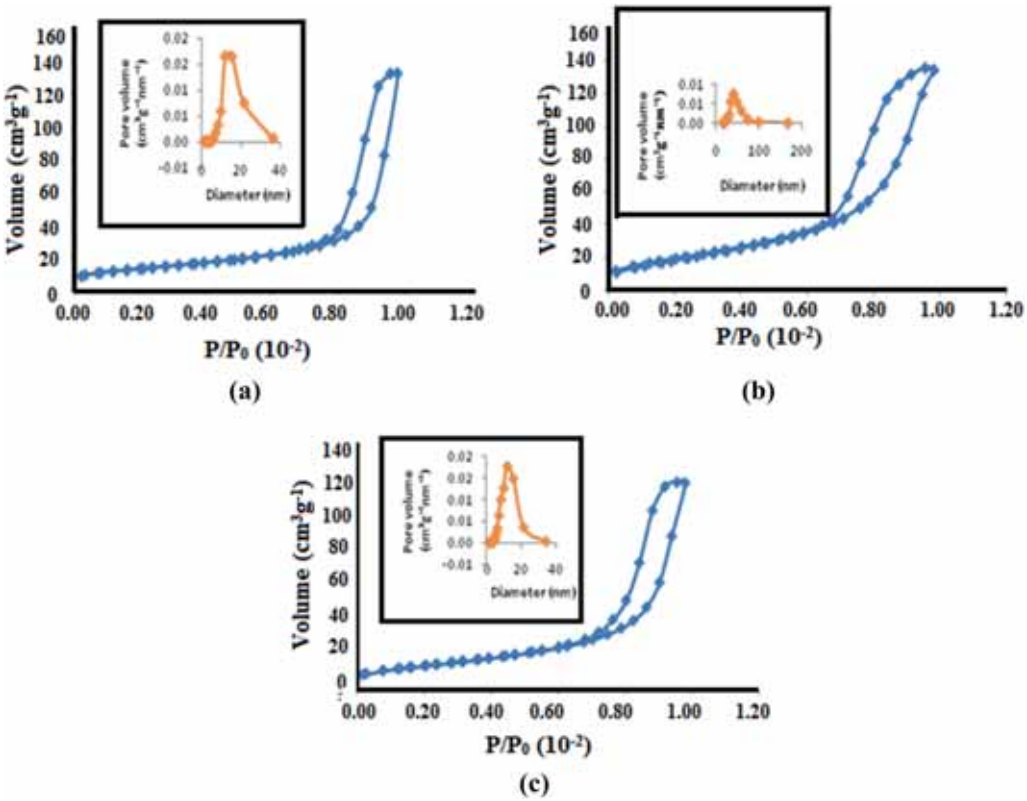

Figure 4. N_2 adsorption isotherms and corresponding pore size distribution (inset) of pristine NPs (F-1) and CTAB-coated Fe_2O_3 NPs (F-2 and F-3).

Table 1. BET surface area parameters of F-1, F-2 and F-3 NPs.

Compound	Surface area ($m^2\ g^{-1}$)	Pore volume ($cm^3\ g^{-1}$)	Pore diameter (nm)
F-1	45.374	0.209	11.971
F-2	69.174	0.218	41.335
F-3	49.072	0.188	12.038

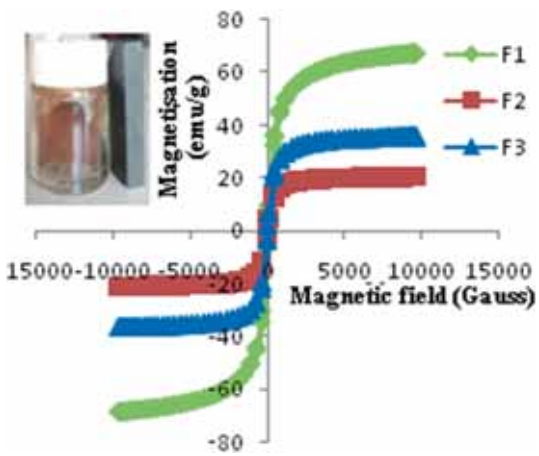

Figure 5. Hysteresis loop of F-1, F-2 and F-3 NPs.

NPs, thus increasing its ability to interact with NPs [40]. Pristine and CTAB-coated Fe_2O_3 NPs could catalyse the oxidation of o-dianisidine dihydrochloride by H_2O_2, producing a dark brown colour. The colour of the CTAB@Fe_2O_3 NPs–H_2O_2–substrate system showed more absorbance than that of the H_2O_2–substrate system, whereas CTAB@Fe_2O_3 NPs–substrate system did not produce any colour (as shown in the inset of figure 6). It indicates that CTAB@Fe_2O_3 NPs possess peroxidase-like activity in the presence of H_2O_2. Also, activity gets enhanced on increasing the substrate concentration because more substrate molecules starts interacting with H_2O_2, thus producing more oxidized product.

The probable mechanism for peroxidase-like activity of CTAB@Fe_2O_3 NPs (1:1) is shown in scheme 1. These NPs catalysed the decomposition of H_2O_2 to produce OH radicals, which furthur oxidized o-dianisidine dihydrochloride, producing dark brown oxidized product.

4.1 *Effect of temperature, contact time and pH on peroxidase mimic activity*

The effect of temperature, contact time and pH on peroxidase mimic activity in the reaction mixture was evaluated.

Table 2. Saturation magnetization, retentivity and coercivity of as-synthesized NPs.

NPs	Saturation magnetization M_s (emu g^{-1})	Retentivity (emu g^{-1})	Coercivity H_c (O_e)
F-1	67.16	482	54.05
F-2	20.12	414	29.59
F-3	35.65	60	12.98

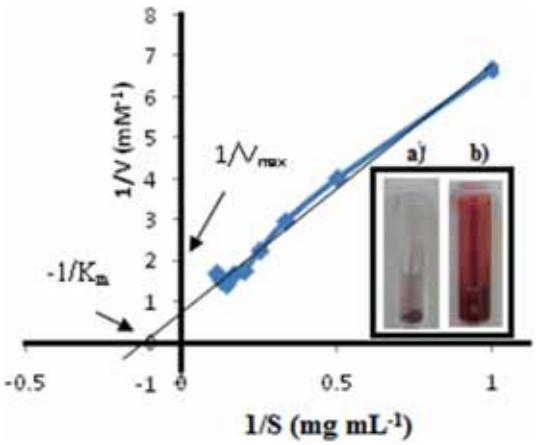

Figure 6. Line-weaver–Burk plot of F-2 NPs (inset—peroxidase-like activity of synthesized NPs: (**a**) CTAB@Fe_2O_3 NPs–substrate system and (**b**) CTAB@Fe_2O_3 NPs–substrate system–H_2O_2 system).

Peroxidase mimic activity of NPs was observed by varying the pH of the reaction mixture from 1 to 10 (figure 7a). The synthesized NPs showed the highest activity at pH 1 and activity decreased on further increasing pH of the reaction mixture. At low pH, the presence of H^+ facilitates the decomposition of H_2O_2, thus increasing the rate of reaction. The variation in temperature from 10 to 45°C resulted in increase in the rate of reaction up to 25°C and later reaction rate showed a decreasing trend, indicating that 25°C was the optimum temperature for peroxidase mimic activity of NPs. The decrease in activity at high temperature can be explained on the basis of reaction mechanism as given in scheme 1. The first step involves the adsorption of H_2O_2 on the surface of NPs followed by the cleavage of H_2O_2 to liberate OH radicals. At high temperature the adsorptive interactions between H_2O_2 and NPs slowed down, leading to decrease in activity [43].

Similarly, concentration of substrate and NPs was optimized by varying their content. Optimum concentration of the substrate was 0.16 mg ml^{-1} and that for F-2 NPs was 1.0 mg ml^{-1} using 0.1 N HCl as solvent (figure 8a). The absorbance of the oxidized product increased with increase in the concentration of F-2 NPs till 1.0 mg ml^{-1} and afterwards it decreased. This was attributed to the aggregation of these particles, which decreased the surface/volume ratio and hence decreased the enzyme mimic activity. Under optimized conditions, peroxidase mimic activities of F-1, F-2 and F-3 were compared. F-2 displayed the highest peroxidase mimic activity followed by F-1 and F-3 (figure 8b). These results suggested that at lower CTAB concentration, activity was increased due to smaller particle size and lesser agglomeration

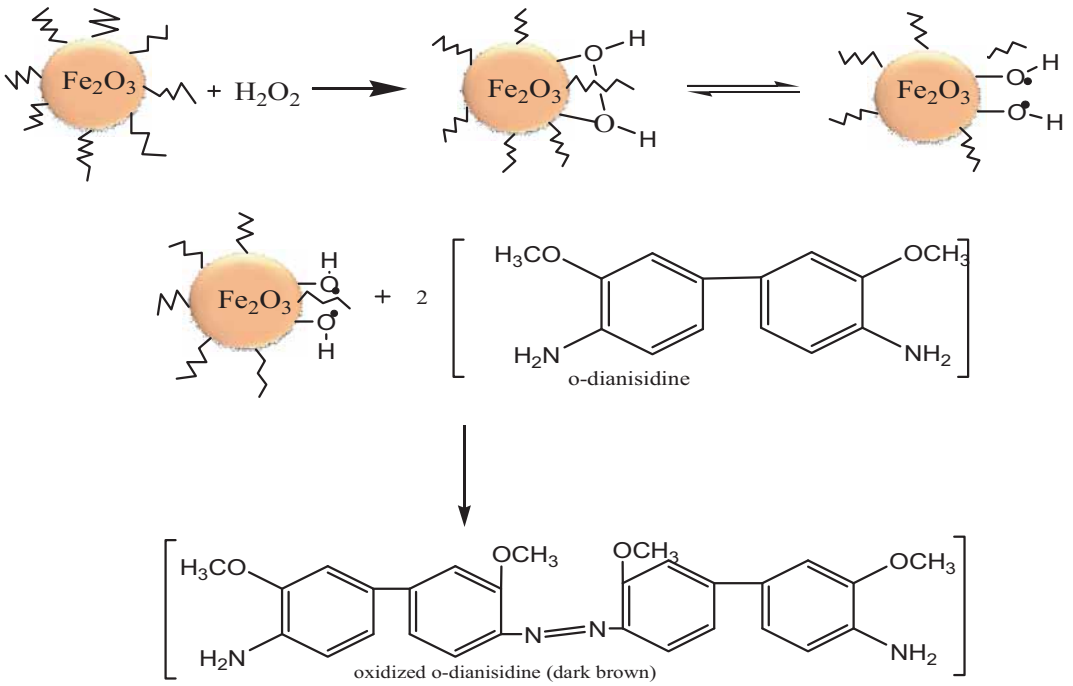

Scheme 1. The mechanism of mimic activity of CTAB@Fe_2O_3 NPs.

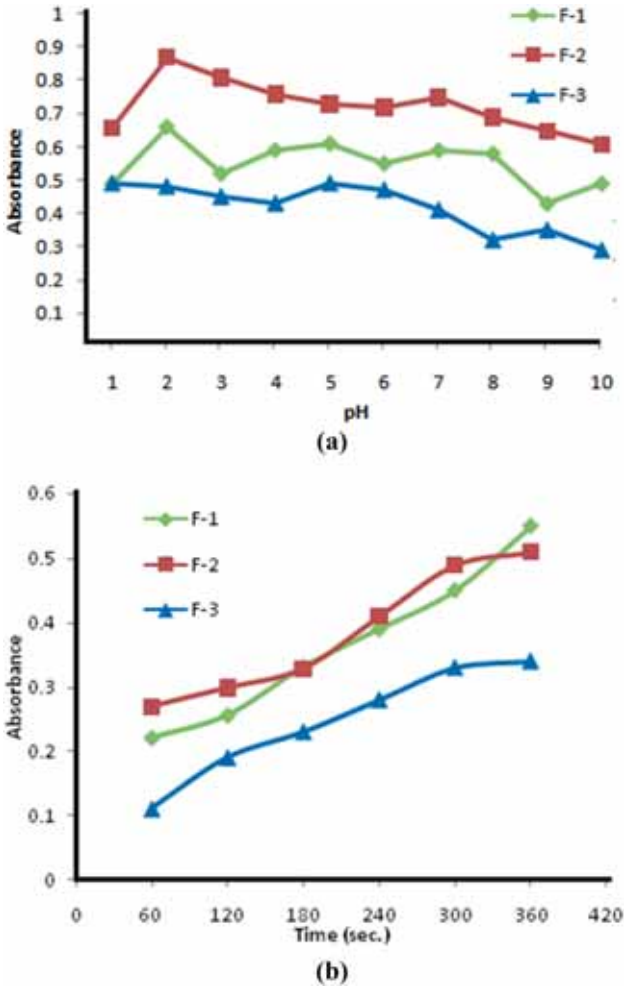

Figure 7. (**a**) Effect of pH on absorbance of solution in the presence of pristine (F-1) and CTAB-coated NPs (F-2 and F-3). (**b**) Effect of time on absorbance of solution using pristine (F-1) and CTAB-coated NPs (F-2 and F-3).

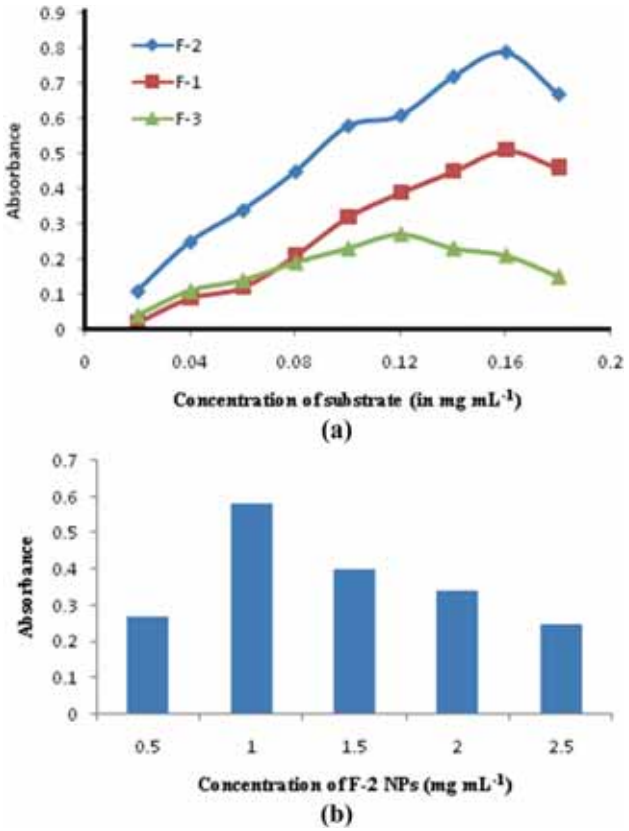

Figure 8. (**a**) Effect of substrate concentration on the absorbance in the presence of pristine (F-1) and CTAB@Fe_2O_3 NPS (F-2 and F-3). (**b**) Graph showing optimized concentration of F-2 NPs.

of NPs, which resulted in greater interaction with substrate. However, at higher CTAB concentration, decrease in peroxidase mimic activity was observed due to steric hindrance by CTAB molecules. The lower surface area of F-3 NPs as compared with F-2 NPs (as confirmed by BET analysis) decreased the number of active sites, thus lowering its interaction with the substrate, and diminished its enzyme mimic activity.

Higher peroxidase mimic activity for the CTAB@Fe_2O_3 NPs was due to the coating, which increased surface area of Fe_2O_3 NPs [44]. Thus, more number of substrate molecules attached to the surface of catalyst due to increase in active sites, which increased turn over number, thus resulting in increased rate of reaction. Another reason for the activity of F-2 NPs was the presence of CTAB, which prevented particles agglomeration, due to which surface of the particles remained free for the substrate to interact. Fe_2O_3 NPs with higher CTAB concentration (1:2) led to decrease in activity due to steric hindrance, which decreased the surface area and thus number of active sites.

4.2 *Kinetic analysis*

Kinetic analysis was performed for the NPs, showing maximum peroxidase mimic activity, i.e., for F-2 NPs. From the Lineweaver–Burk plot (figure 6), the calculated K_m and V_{max} values of F-2 NPs are 7.69 mM and 1.12 μmol s^{-1}, respectively. Savitsky *et al* [45] also studied the kinetic analysis of o-dianisidine oxidation using free and antibody complexes of iron(lll) coproporphyrin as peroxidase mimic. The K_m obtained for various complexes are in the range 0.53–5.9 $\times 10^6$ M, whereas in the present study the K_m value is much lower, which confirms higher affinity of CTAB@Fe_2O_3 NPs for the substrate. Lower value of K_m is an essential parameter for potential activity of enzyme mimics. Thus, kinetic studies authenticated the promising peroxidase mimic activity of CTAB@Fe_2O_3 NPs having w/w ratio 1:1.

5. Conclusion

We have synthesized pristine and CTAB-coated ferric oxide NPs (CTAB@Fe_2O_3 NPs) by co-precipitation method and

compared their peroxidase mimic activity. Results showed that Fe_2O_3 NPs synthesized in the presence of CTAB having w/w ratio of 1:1 displayed higher peroxidase mimic activity, which was correlated with the higher surface area of the NPs. Further increase in CTAB concentration resulted in decrease in activity due to steric hindrance by the CTAB molecules adhering on the surface of NPs. CTAB@Fe_2O_3 NPs as peroxidase mimic showed promising properties, viz., easy preparation, storage, reusability, stability, dispersibility and easy separation, as compared with natural enzymes. They can be explored for varied applications as an economically viable substitute to peroxidase enzyme in various practical bio-medical applications such as biosensors for the detection of hydrogen peroxide in various commodities and glucose level in blood.

Acknowledgements

We are grateful to EMN Lab of Punjab Agricultural University, Ludhiana, for SEM and TEM recordings.

References

[1] Shoji E and Freund M S 2001 *J. Am. Chem. Soc.* **123** 3383
[2] Breslow R 1995 *Acc. Chem. Res.* **28** 146
[3] Wei H and Wang E 2013 *Chem. Soc. Rev.* **42** 6060
[4] Colombo M, Carregal R S, Casula M F, Gutierrez L, Morales M P, Bohm I B *et al* 2012 *Chem. Soc. Rev.* **41** 4306
[5] Chen W, Chen J, Feng Y B, Hong L, Chen Q Y, Wu L F *et al* 2012 *Analyst* **137** 1706
[6] Chen Z, Yin J J, Zhou Y T, Zhang Y, Song L, Song M *et al* 2012 *ACS Nano* **6** 4001
[7] Cui R, Han Z and Zhu J J 2011 *Chem. Eur. J.* **17** 9377
[8] Song Y, Qu K, Zhao C, Ren J and Qu X 2010 *Adv. Mater.* **22** 2206
[9] Zheng A X, Cong Z X, Wang J R, Li J, Yang H H and Chen G N 2013 *Biosens. Bioelectron.* **49** 519
[10] Bi S, Zhao T, Jia X and He P 2014 *Biosens. Bioelectron.* **57** 110
[11] Xing Z, Tian J, Asiri A M, Qusti A H, Al Youbi A O and Sun X 2014 *Biosens. Bioelectron.* **52** 452
[12] Jiang H, Chen Z, Cao H and Huang Y 2012 *Analyst* **137** 5560
[13] Jv Y, Li B and Cao R 2010 *Chem. Commun.* **46** 8017
[14] Andre R, Natalio F, Humanes M, Leppin J, Heinze K, Wever R *et al* 2011 *Adv. Funct. Mater.* **21** 501
[15] Chen W, Chen J, Liu A L, Wang L M, Li G W and Lin X H 2011 *Chem. Cat. Chem.* **3** 1151
[16] Mu J, Wang Y, Zhao M and Zhang L 2012 *Chem. Commun.* **48** 2540
[17] Gao L Z, Zhuang J, Nie L, Zhang J B, Zhang Y, Gu N *et al* 2007 *Nat. Nanotechnol.* **2** 577
[18] Henriksen A, Smith A T and Gajhede M 1999 *J. Biol. Chem.* **274** 35005
[19] Kvaratskhelia M, Winkel C and Thorneley R N F 1997 *Plant Physiol.* **114** 1237
[20] Kariya K, Lee E, Hirouchi M, Hosokawa M and Sayo H 1987 *Biochim. Biophys. Acta* **911** 95
[21] Hartert M M, Bourgeois E, Grülke S, Dupont G D, Caudron I, Deby C *et al* 1998 *Can. J. Vet. Res.* **62** 127
[22] Yu F, Huang Y, Cole A J and Yang V C 2009 *Biomaterials* **30** 4716
[23] Clement O, Siauve N, Cuenod C A and Frija G 1998 *Top. Magn. Reson. Imaging* **9** 167
[24] Johnson L, Pinder S E and Douek M 2013 *Histopathology* **62** 481
[25] Kernstine K H, Stanford W and Mullan B F 1999 *Ann. Thorac. Surg.* **68** 1022
[26] Harisinghani M G, Saini S, Hahn P F, Weissleder R and Mueller P R 1998 *Acad. Radiol.* **5** 167
[27] Reimer P and Balzer T 2003 *Eur. Radiol.* **13** 1266
[28] Vogl T J, Hammersting l R and Schwarz W 1996 *Invest. Radiol.* **31** 696
[29] Reimer P, Rummeny E J and Daldrup H E 1995 *Radiology* **195** 489
[30] Bonnemain B 1998 *J. Drug Target.* **6** 167
[31] Campbell J L, Arora J, Cowell S F, Garg A, Eu P, Bhargava S K *et al* 2011 *PLoS One* **6** 21857
[32] Bullivant J P, Zhao S, Willenberg B J, Kozissnik B, Batich C D and Dobson J 2013 *Int. J. Mol. Sci.* **14** 17501
[33] Zhang Y, Xu D, Li W, Yu J and Chen Y 2012 *J. Nanomater.* **2012** 1
[34] Qiu Y, Liu Y, Wang L, Xu L, Bai R, Ji Y *et al* 2010 *Biomaterials* **31** 7606
[35] Deng J H, Zhang X R, Zeng G M, Gong J L, Niu Q Y and Liang J 2013 *Chem. Eng. J.* **226** 189
[36] Grewal J K and Kaur M 2017 *Ceram. Int.* **43** 16611
[37] Shannon L M, Kay E and Lew J Y 1966 *J. Biol. Chem.* **241** 2166
[38] Uzunov I and Aleksandrova A 2002 *Chem. Inorg.* **62** 195
[39] Hoan N T V, Thu N T A, Duc H V, Cuong N D, Khieu D Q and Vo V 2016 *J. Chem.* **2016** 1
[40] Zhao B and Nan Z 2011 *Nanoscale Res. Lett.* **6** 1
[41] Chen A, Wang H, Zhao B and Li X 2003 *Synth. Met.* **139** 411
[42] Ubhi M K, Kaur M, Singh D and Granchee J M 2017 *Pure Appl. Chem.* **11** 247
[43] Johnson B B 1990 *Environ. Sci. Technol.* **24** 112
[44] Cai S, Jia X, Han Q, Yan X, Yang R and Wang C 2017 *Nano Res.* **10** 2056
[45] Savitsky A P, Nelen M I, Yatsmirsky A K, Demcheva M V, Ponomarev G V and Nikov I V 1994 *Appl. Biochem. Biotechnol.* **47** 317